Nodal densities of Gaussian random waves satisfying mixed boundary conditions

2002 J. Phys. A: Math. Gen. 35 5961

(http://iopscience.iop.org/0305-4470/35/29/302)

INSTITUTE OF PHYSICS PUBLISHING JOURNAL OF PHYSICS A: MATHEMATICAL AND GENERAL

J. Phys. A: Math. Gen. **35** (2002) 5961–5972 PII: S0305-4470(02)36195-X

Nodal densities of Gaussian random waves satisfying mixed boundary conditions

M V Berry[1] **and H Ishio**[2]

[1] H H Wills Physics Laboratory, Tyndall Avenue, Bristol BS8 1TL, UK
[2] School of Mathematics, University of Bristol, University Walk, Bristol BS8 1TW, UK

Received 24 April 2002
Published 12 July 2002
Online at stacks.iop.org/JPhysA/35/5961

Abstract

Nodal statistics are derived for 'boundary-adapted Gaussian random waves' $\psi = u + \mathrm{i}v$ in the plane, satisfying the Helmholtz equation and mixed boundary conditions, in which a linear combination of ψ and its normal derivative, characterized by a parameter a, vanishes on a line. For both the density of nodal lines for $\mathrm{Re}\,\psi = u$ and the density of nodal points for complex ψ, effects of the boundary persist, surprisingly, infinitely far from the boundary, and, also surprisingly, are independent of a. As a increases from the Dirichlet value $a = 0$, nodal line and point structures migrate from the boundary, and can be described analytically.

PACS numbers: 02.50.−r, 03.65.Sq, 05.45.Mt

1. Introduction

A widely-discussed class of Gaussian random functions of two variables $\mathbf{R} = \{X, Y\} = \{kx, ky\}$ consists of superpositions of plane waves travelling in different directions but with the same wavelength $\lambda = 2\pi/k$. These are models for confined quantum waves associated with classically chaotic trajectories, for example, eigenfunctions in ergodic quantum billiards (Berry 1977, O'Connor *et al* 1987, Heller 1991, Saichev *et al* 2002, Blum *et al* 2002). The waves are real if the system has time-reversal symmetry (T) and complex otherwise. In a recent improvement of the model (Berry 2002, hereinafter called I), 'boundary-adapted Gaussian random waves' were constructed to satisfy Dirichlet or Neumann boundary conditions along a straight line, chosen as $Y = 0$. For these waves, some statistics of nodal lines (with T) and points (without T) were calculated, revealing interesting Y-dependence.

Our aim here is to generalize this improvement to boundary-adapted Gaussian random waves satisfying the family of mixed conditions

$$\psi(X, 0; a)\cos a + \psi_Y(X, 0; a)\sin a = 0 \qquad \left(-\tfrac{1}{2}\pi < a \leqslant \tfrac{1}{2}\pi\right). \tag{1}$$

Here and hereafter, italic subscripts denote derivatives, and a is a parameter labelling members of the family; for Dirichlet conditions, $a = 0$, while for Neumann $a = \pi/2$. This family of

relations between the wavefunction and its normal derivative is a special case of the Robin boundary condition (Gustavson and Abe 1998). The generalization has more than technical interest, since associated with it are two unanticipated phenomena that we wish to draw attention to. First, the long-range depletion (for nodal lines) and enhancement (for nodal points) of nodal densities, already noted in I for Dirichlet and Neumann conditions, persist (section 2) independent of the parameter a. Second, for a small and positive there is a rich nodal structure for small Y (section 3), which can be regarded as a 'ghost of the departed Dirichlet nodal line' that exists at $Y = 0$ when $a = 0$, and can be described analytically.

As a short calculation confirms, the Gaussian random superposition of complex waves ψ, with real and imaginary parts u and v, satisfying the Helmholtz equation and the boundary condition (1), can be written as

$$\psi(\mathbf{R};a) \equiv u(\mathbf{R};a) + \mathrm{i}v(\mathbf{R};a)$$
$$= \frac{2}{\sqrt{J}} \sum_{j=1}^{J} \frac{[\sin(Y\sin\theta_j) - \tan a \sin\theta_j \cos(Y\sin\theta_j)]}{\sqrt{1+\tan^2 a \sin^2\theta_j}} \exp(\mathrm{i}(X\cos\theta_j + \phi_j)). \quad (2)$$

This consists of J ($\gg 1$) waves travelling in directions θ_j, equidistributed on the range $[0, \pi]$, with phases ϕ_j, equidistributed on the range $[0, 2\pi]$. Figure 1 shows three plots of a sample function ψ of this type, for $a = \pi/4$, indicating the nodal lines for the real part u of the wave and the nodal points of ψ (intersections of nodal lines of u and v).

2. Nodal densities

We will calculate the density $\rho_{\mathrm{L}}(Y;a)$ of nodal lines for real waves $u(\mathbf{R};a)$, and the density $\rho_{\mathrm{P}}(Y;a)$ of nodal points for complex waves $\psi(\mathbf{R};a)$, both quantities being scaled so that $\rho \to 1$ as $Y \to \infty$. The techniques are identical to those in I (see also Berry and Dennis 2000), involving certain averages over the ensemble of random waves. The only new feature is that these averages depend on a, and cannot be expressed compactly in terms of Bessel functions as in the Dirichlet and Neumann cases.

The relevant averages (the same for the real and imaginary parts u and v, which are also statistically independent) are easily calculated as

$$\begin{aligned}
B(Y;a) &\equiv \langle u^2 \rangle = 1 - \frac{2}{\pi}\int_0^{\pi/2} \mathrm{d}\theta \frac{f_1(\theta;a)}{1+\tan^2 a \sin^2\theta} \\
D_X(Y;a) &\equiv \langle u_X^2 \rangle = \frac{1}{2} - \frac{2}{\pi}\int_0^{\pi/2} \mathrm{d}\theta \cos^2\theta \frac{f_1(\theta;a)}{1+\tan^2 a \sin^2\theta} \\
D_Y(Y;a) &\equiv \langle u_Y^2 \rangle = D_X(Y;a) - B(Y;a) + 1 \\
K(Y;a) &\equiv \langle u u_Y \rangle = \frac{2}{\pi}\int_0^{\pi/2} \mathrm{d}\theta \sin\theta \frac{f_2(\theta;a)}{1+\tan^2 a \sin^2\theta}
\end{aligned} \quad (3)$$

where

$$\begin{aligned}
f_1(\theta;a) &\equiv [(1-\tan^2 a \sin^2\theta)\cos(2Y\sin\theta) + 2\tan a \sin\theta \sin(2Y\sin\theta)] \\
f_2(\theta;a) &\equiv [(1-\tan^2 a \sin^2\theta)\sin(2Y\sin\theta) - 2\tan a \sin\theta \cos(2Y\sin\theta)].
\end{aligned} \quad (4)$$

For economy of notation, we will frequently not indicate the variables explicitly, and refer simply to B, D_X, etc.

For real waves, the nodal density to be calculated is $\rho_{\mathrm{L}}(Y;a)$, defined by

$$\langle \text{line length per unit area} \rangle = \frac{k}{2\sqrt{2}} \rho_{\mathrm{L}}(Y;a) \quad (5)$$

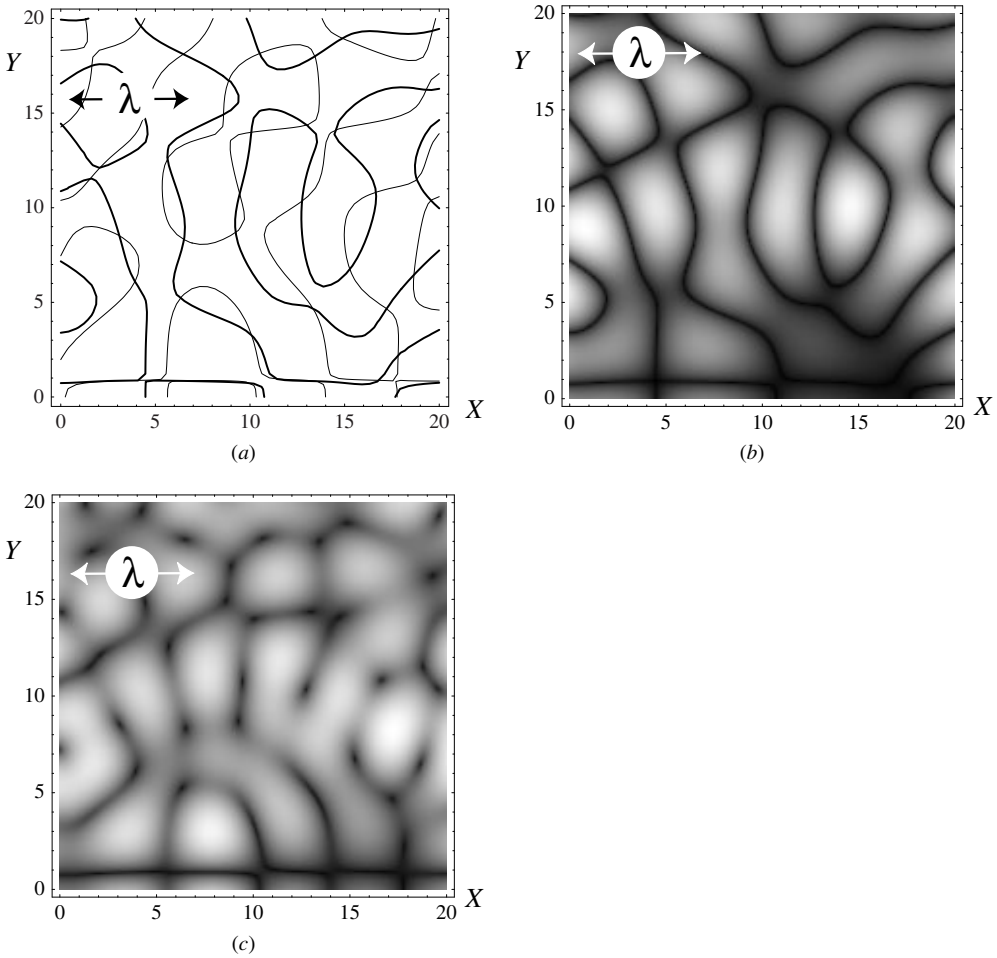

Figure 1. Samples of a Gaussian random function ψ with $J = 287$ plane waves, for boundary-condition parameter $a = \pi/4$. (*a*) Nodal lines of $u = \mathrm{Re}\,\psi$ (thick) and $v = \mathrm{Im}\,\psi$ (thin), with nodal points of ψ indicated by intersections of the nodal lines; (*b*) density plot of u, with nodal lines black; (*c*) density plot of $|\psi|$, with nodal points black. The wavelength λ is indicated.

incorporating the previously derived bulk density $k/(2\sqrt{2})$ for nodal lines of isotropic Gaussian random functions far from boundaries. Application of identical reasoning to that in I leads to

$$\rho_{\mathrm{L}}(Y;a) = \frac{2\sqrt{2}}{\pi} D_X \left(BD_Y - K^2\right) \int_0^{\pi/2} \frac{\mathrm{d}\theta}{\left(BD_X \cos^2\theta + \left(BD_Y - K^2\right)\sin^2\theta\right)^{3/2}}$$
$$= \frac{2}{\pi}\sqrt{\frac{2D_X}{B}}\, E\left(\frac{B(B-1)+K^2}{BD_X}\right) \tag{6}$$

where in the second equality (not given previously) E denotes the complete elliptic integral (the definition is that of *Mathematica* (Wolfram 1996)).

Figure 2 shows nodal line densities for several values of a, in excellent agreement with numerically-computed ensemble averages over sample waves of type (2). The peak for $a = \pi/4$ will be discussed in detail in section 3.

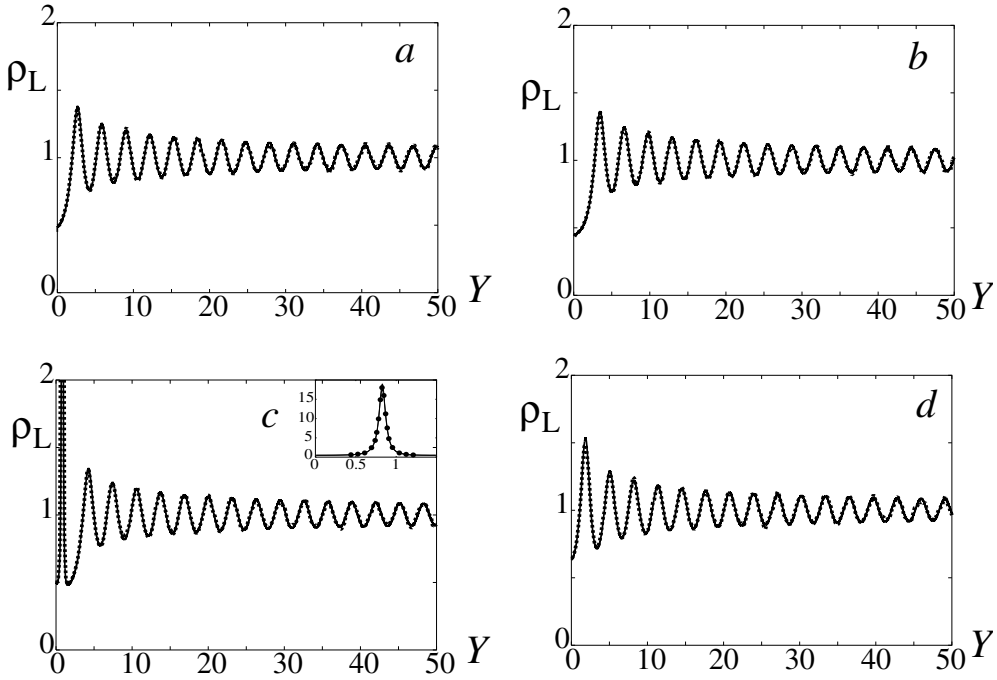

Figure 2. Nodal line densities $\rho_{\mathrm{L}}(Y;a)$, for $(a)\ a=-\pi/4$, $(b)\ a=0$, $(c)\ a=+\pi/4$, $(d)\ a=+\pi/2$. Thick curves: theoretical formula (6); dotted curves: averages over 25 numerically computed Gaussian random functions each made from $J=287$ plane waves. The inset is a magnification of the small-Y peak, with the points being numerical averages.

For complex waves, the nodal density to be calculated is $\rho_{\mathrm{P}}(Y;a)$, defined by

$$\langle\text{number of nodal points per unit area}\rangle = \frac{k^2}{4\pi}\rho_{\mathrm{P}}(Y;a) \tag{7}$$

incorporating the previously derived (Berry and Robnik 1986) bulk density $k^2/(4\pi)$ for nodal points of isotropic Gaussian random functions far from boundaries. Application of identical reasoning to that in I leads to

$$\rho_{\mathrm{P}}(Y;a) = \frac{2\sqrt{D_X\left(BD_Y - K^2\right)}}{B^{3/2}}. \tag{8}$$

Figure 3 shows nodal point densities for several values of a, again in good agreement with numerically-computed ensemble averages over sample waves of type (2). The peak for $a=\pi/4$ will be discussed in detail in section 3.

The long-range behaviour of the nodal densities can be established from the asymptotic behaviour of correlations (3) and expressions (6) and (8). Straightforward but long calculations lead to

$$\rho_{\mathrm{L}}(Y;a) \approx 1 + \frac{\cos\left(2Y-2a-\frac{1}{4}\pi\right)}{\sqrt{\pi Y}} - \frac{1}{32\pi Y} \qquad (Y\gg 1) \tag{9}$$

and

$$\rho_{\mathrm{P}}(Y;a) \approx 1 + \frac{2\cos\left(2Y-2a-\frac{1}{4}\pi\right)}{\sqrt{\pi Y}} + \frac{1}{4\pi Y} \qquad (Y\gg 1). \tag{10}$$

Figures 4 and 5 show how accurately these asymptotic formulae describe the densities, even for rather small Y.

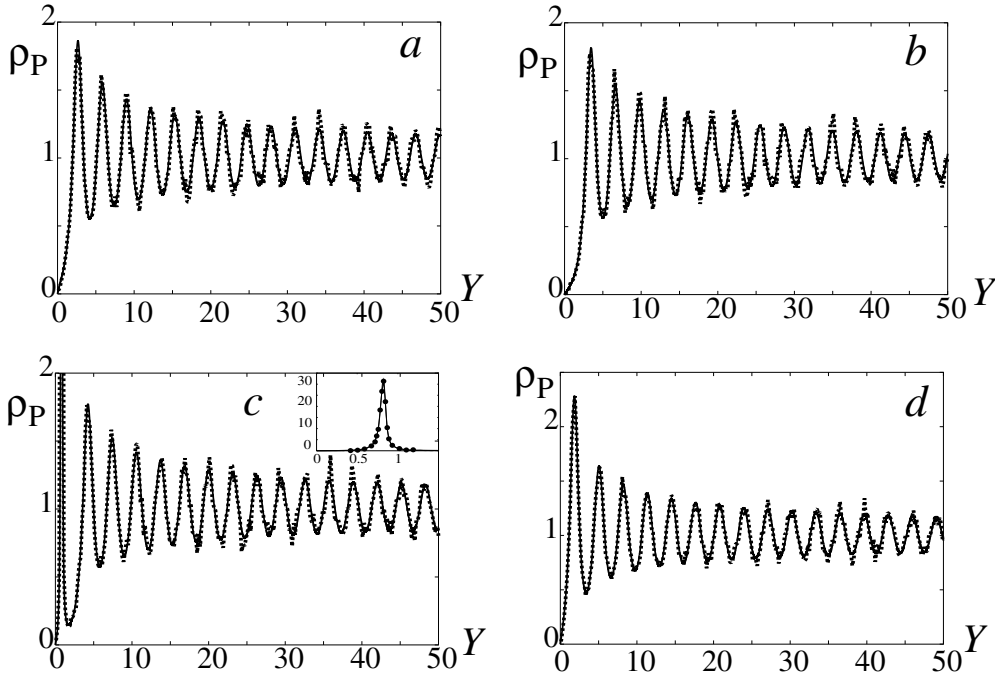

Figure 3. As figure 2, for nodal point densities $\rho_{\mathrm{P}}(Y;a)$ and the theoretical formula (8).

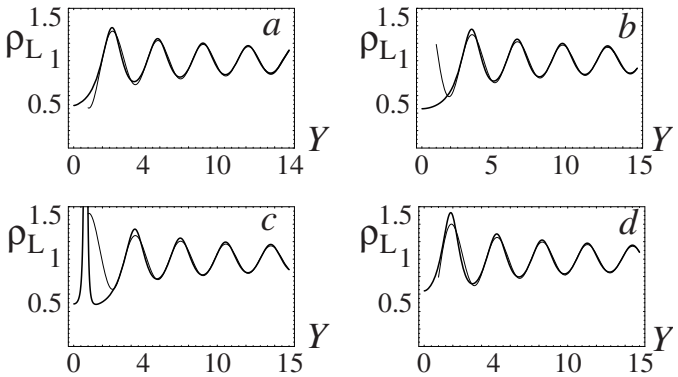

Figure 4. As figure 2, with the thin curves showing the asymptotic formula (9).

The most striking aspect of the large-Y asymptotics is the Y^{-1} dependence of the leading nonoscillatory correction. This means that when the excess $\rho - 1$ is integrated to give the mean excess length of nodal line or number of nodal points in a strip of height Y, the result diverges as $Y \to \infty$. Thus

$$L_{\mathrm{exc}}(Y;a) \equiv \int_0^Y \mathrm{d}\eta(\rho_{\mathrm{L}}(\eta;a)-1)$$
$$= \frac{\sin\left(2Y-2a-\frac{1}{4}\pi\right)}{2\sqrt{\pi Y}} - \frac{\log Y}{32\pi} + C_{\mathrm{L}}(a) \qquad (Y \gg 1) \qquad (11)$$

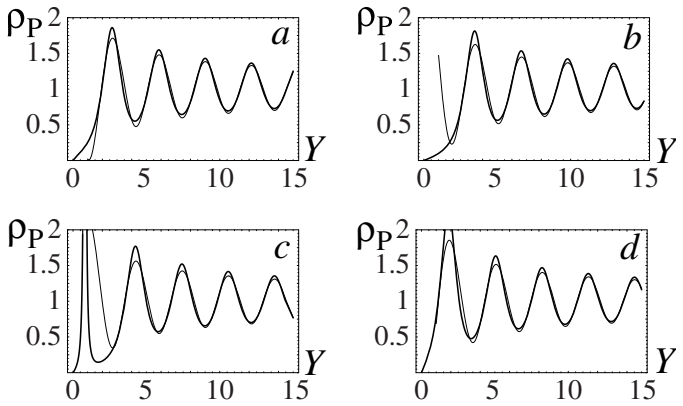

Figure 5. As figure 3, with the thin curves showing the asymptotic formula (10).

and

$$N_{\rm exc}(Y;a) \equiv \int_0^Y {\rm d}\eta(\rho_{\rm P}(\eta;a)-1)$$
$$= \frac{\sin\left(2Y-2a-\frac{1}{4}\pi\right)}{\sqrt{\pi Y}} + \frac{\log Y}{4\pi} + C_{\rm P}(a) \qquad (Y \gg 1) \tag{12}$$

where the numerically-determined constants $C_{\rm L}$ and $C_{\rm P}$ are shown in figures 12 and 13 and will be discussed later.

These divergences imply that there is a sense in which the effect of the boundary conditions persists infinitely far from the boundary, a fact whose implications for quantum billiards were discussed in I. Moreover, the coefficients of the logarithmic terms are the same for all values of the boundary parameter a, implying that, surprisingly, the nature of the divergence resulting from the imposition of boundary conditions on Gaussian random functions is independent of the form of the boundary condition. Figures 6 and 7 show how well these logarithmic divergences describe the ensemble averages over numerically-computed random waves.

3. Ghosts of the departed Dirichlet nodal line

Now we concentrate on the small-Y peaks in figures 2(c) and 3(c), corresponding to $a = \pi/4$, and show that these reflect migrated remnants of the nodal line (for both real and complex waves) at $Y = 0$ for the Dirichlet case $a = 0$.

For a small and Y close to a, wave (2) can be expanded in a series whose leading terms are

$$\psi(\mathbf{R};a) \approx \left(Y-a-\tfrac{1}{3}a^3\right)\,(u_1(X)+{\rm i}v_1(X)) - \tfrac{1}{3}a^3(u_3(X)+{\rm i}v_3(X)) \tag{13}$$

where we employ the notation

$$u_1(X) \equiv u_Y(X,0;0) \qquad u_3(X) \equiv u_{YYY}(X,0;0) \tag{14}$$

to denote odd normal derivatives of the Dirichlet wave on the boundary, and similarly for v. Equating ψ to zero gives, for real waves, the nodal line whose equation is

$$Y = a + \frac{1}{3}a^3\left(1+\frac{u_3(X)}{u_1(X)}\right). \tag{15}$$

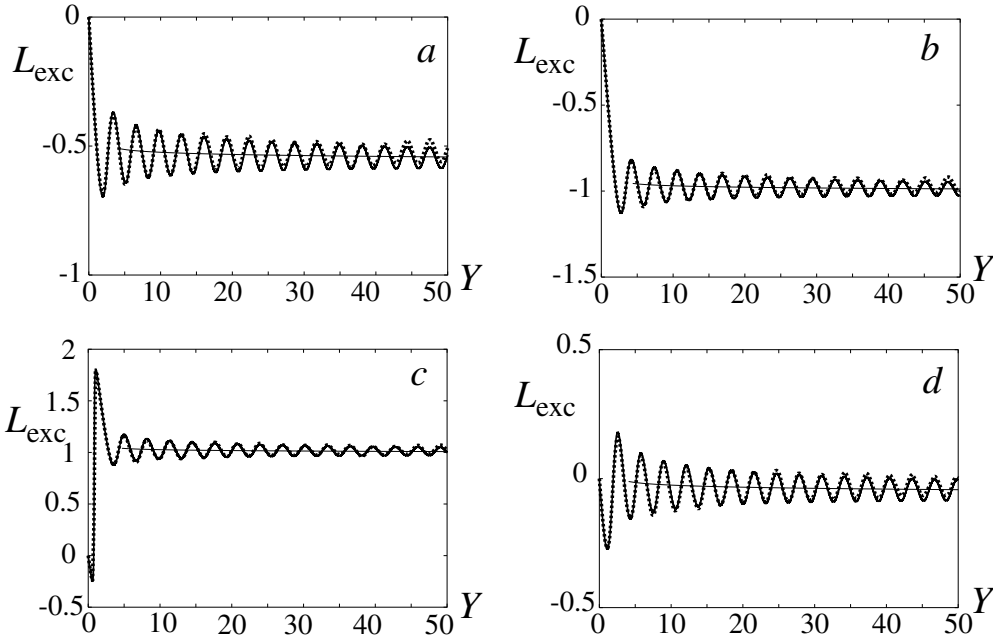

Figure 6. As figure 2, for the excess line density $L_{\rm exc}(Y;a)$, with the fine line showing the smoothed asymptotics $-\log Y/32\pi + C_{\rm L}(a)$.

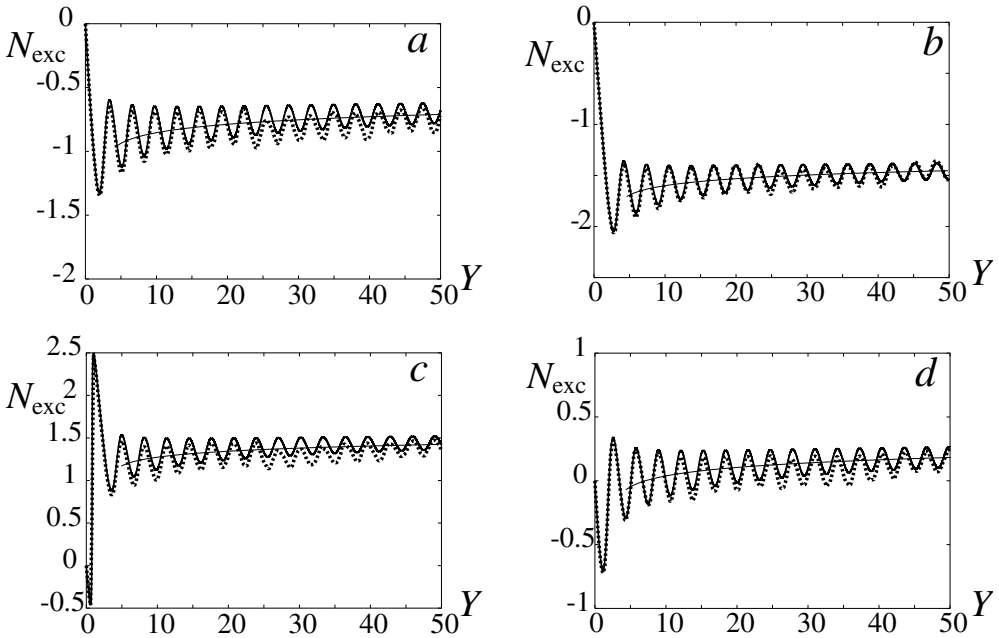

Figure 7. As figure 3, for the excess point density $N_{\rm exc}(Y;a)$, with the fine line showing the smoothed asymptotics $+\log Y/4\pi + C_{\rm P}(a)$.

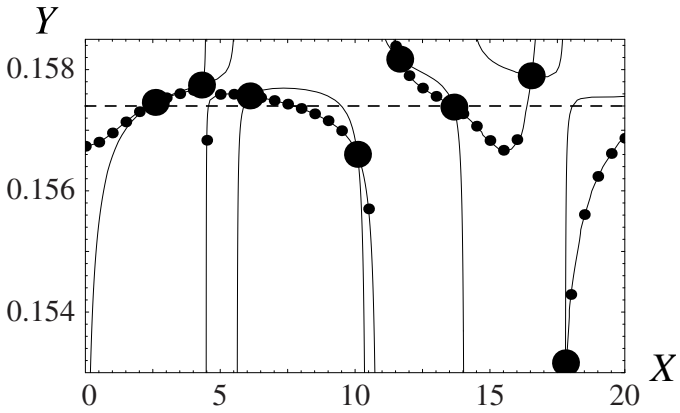

Figure 8. Nodal lines of u and v for a sample Gaussian random function with $a = \pi/20 = 0.157\,07$. Small dots: theoretical formula (15) for nodal lines of u; large dots: theoretical formula (16) for nodal points of ψ; dashed line: $Y = a + a^3/12$.

For complex waves the nodal points $\{X, Y\}$ are the simultaneous solutions of

$$\left.\begin{aligned} Y &= a + \frac{1}{3}a^3\left(1 + \operatorname{Re}\left\{\frac{\psi_3(X)}{\psi_1(X)}\right\}\right) \\ &= a + \frac{1}{3}a^3\left(1 + \frac{u_1(X)\,u_3(X) + v_1(X)\,v_3(X)}{u_1^2(X) + v_1^2(X)}\right) \\ \operatorname{Im}\left\{\frac{\psi_3(X)}{\psi_1(X)}\right\} &= 0 \qquad \text{i.e.} \quad u_3(X)v_1(X) - u_1(X)\,v_3(X) = 0 \end{aligned}\right\}. \tag{16}$$

Two implications of these equations are: a nodal structure close to $Y = a$, and therefore part of the physical wave $Y > 0$ when a is positive; and concentration of this nodal structure within a strip whose Y-width is of order a^3—that is, the peaks get sharper as a gets smaller. Figure 8 illustrates how accurately this small-a asymptotic theory describes the nodal lines and points for an individual function from the ensemble (2).

To determine the shape of the small-a peaks, it is convenient to measure Y from a, in units of a^3, defining η by

$$Y \equiv a + a^3\eta \tag{17}$$

and expanding averages (3) for small a. To the lowest relevant order, this gives

$$\left.\begin{aligned} B &\approx a^6\left(\left(\eta - \tfrac{1}{12}\right)^2 + \tfrac{1}{144}\right) \\ D_X &\approx \tfrac{1}{4}a^6\left(\left(\eta - \tfrac{1}{6}\right)^2 + \tfrac{1}{144}\right) \\ D_Y &\approx 1 \\ K &\approx -\tfrac{1}{12}a^3(1 - 12\eta) \end{aligned}\right\} \qquad (a \ll 1). \tag{18}$$

For the nodal line density, substitution into (6), and further expansion, gives the Lorentzian peak shape

$$\rho_{\mathrm{L}}(a + a^3\eta;\, a) \approx \frac{24\sqrt{2}}{\pi a^3(1 + (12\eta - 1)^2)} \qquad (a \ll 1) \tag{19}$$

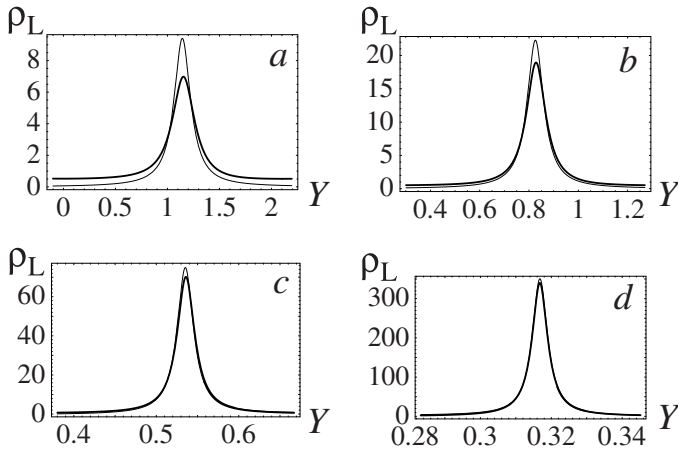

Figure 9. Small-Y peaks in $\rho_{\mathrm{L}}(Y; a)$, for (a) $a = \pi/3$, (b) $a = \pi/4$, (c) $a = \pi/6$, (d) $a = \pi/10$. Thick curves: exact formula (6); thin curves: asymptotic formula (19).

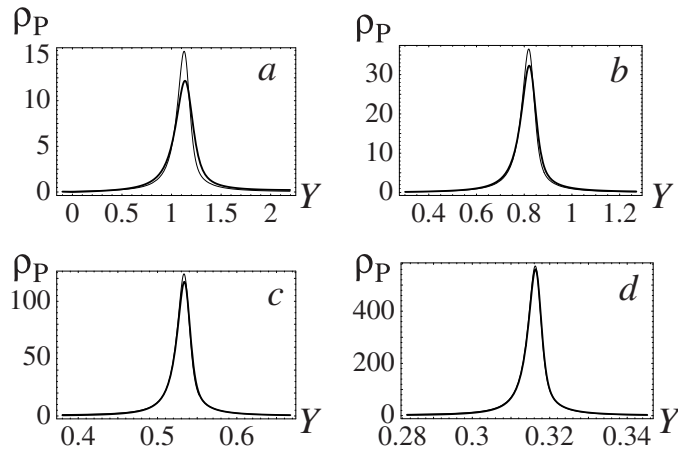

Figure 10. As figure 9, for $\rho_{\mathrm{P}}(Y; a)$, with the exact formula (8) and the asymptotic formula (20).

with a maximum at $\eta = 1/12$, that is $Y = a + a^3/12$. As figure 9 shows, this gives an increasingly accurate description of the peaks as a decreases. For the nodal point density, substitution into (8) gives the distorted Lorentzian peak shape

$$\rho_{\mathrm{P}}(a + a^3\eta; a) \approx \frac{12\sqrt{1 + (12\eta - 2)^2}}{a^3(1 + (12\eta - 1)^2)^{3/2}} \qquad (a \ll 1) \tag{20}$$

with a maximum close to $\eta = 1/12$ (actually $\eta = 1/12 - 0.004\,598$). As figure 10 shows, this is accurate for small a too.

The heights of the peaks scale as a^{-3}, with coefficients

$$\rho_{\mathrm{L}}\left(a + \frac{1}{12}a^3; a\right) \approx \frac{24\sqrt{2}}{\pi a^3} \qquad (a \ll 1) \tag{21}$$

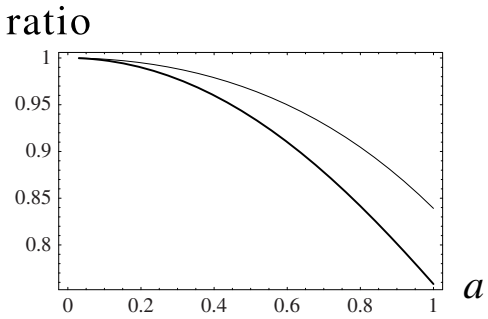

Figure 11. Nodal densities at $Y = a + a^3/12$, close to the maximum for small a. Thick curve, ratio ρ_{L}/theoretical value (21); thin curve, ratio ρ_{P}/theoretical value (22).

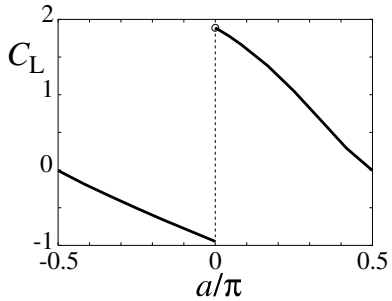

Figure 12. Constant $C_{\mathrm{L}}(a)$ in the excess nodal line asymptotics (11).

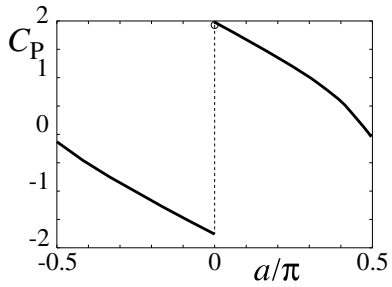

Figure 13. Constant $C_{\mathrm{P}}(a)$ in the excess nodal point asymptotics (12).

and

$$\rho_{\mathrm{P}}\left(a + \frac{1}{12}a^3; a\right) \approx \frac{12\sqrt{2}}{a^3} \qquad (a \ll 1). \tag{22}$$

Figure 11 shows the accuracy of these formulae.

For negative a, these nodal density peaks lie on the negative-Y (virtual) side of the field. As a increases through zero, the peaks appear as δ-function contributions at $Y = 0$. Therefore the integrals of the nodal densities—the nodal excesses (11) and (12)—are discontinuous at $a = 0$, so the asymptotic constants $C_{\mathrm{L}}(a)$ and $C_{\mathrm{P}}(a)$ are discontinuous at $a = 0$. The constants are shown in figures 12 and 13.

For nodal lines, (19) gives the discontinuity as

$$\Delta C_{\mathrm{L}} \equiv \lim_{a\to 0_+}(C_{\mathrm{L}}(a) - C_{\mathrm{L}}(-a)) = \lim_{a\to 0_+} a^3 \int_{-\infty}^{\infty} \mathrm{d}\eta\, \rho_{\mathrm{L}}(a + a^3\eta;\ a) \ = \ 2\sqrt{2}. \tag{23}$$

The correctness of this result is immediately confirmed by the observation that the line appearing from $a = 0$ is simply the Dirichlet nodal line along the Y-axis, whose length per unit X-width is of course unity, which after the scaling (5) is $2\sqrt{2}$.

For nodal points, (20) gives the discontinuity as

$$\Delta C_{\mathrm{P}} \equiv \lim_{a\to 0_+}(C_{\mathrm{P}}(a) - C_{\mathrm{P}}(-a)) = \lim_{a\to 0_+} a^3 \int_{-\infty}^{\infty} \mathrm{d}\eta\, \rho_{\mathrm{P}}(a + a^3\eta;\ a)$$
$$= (\sqrt{5}-1)\, E\left(\frac{1}{4}\pi, -\frac{\sqrt{5}}{2}(\sqrt{5}+3)\right)$$
$$+ (\sqrt{5}+1) E\left(\frac{1}{4}\pi, \frac{\sqrt{5}}{2}(-\sqrt{5}+3)\right) = 3.690\,34. \tag{24}$$

Here E denotes the incomplete elliptic integral (the definition is that of *Mathematica* (Wolfram 1996)). An alternative way to confirm the correctness of this result is to calculate the mean X-density of the nodal points as given by the second equation in (16), after the scaling (7):

$$\Delta C_{\mathrm{P}} = 4\pi \langle \delta(u_3 v_1 - u_1 v_3) |\partial_X (u_3 v_1 - u_1 v_3)| \rangle. \tag{25}$$

A lengthy calculation reproduces (24).

4. Discussion

We have explored several ways in which boundary conditions along a line affect the statistical properties of Gaussian random functions. Two unexpected phenomena emerged from this study. First, the effects of the boundary persist infinitely far from the boundary, and are independent of the form of the boundary condition: the long-range nodal line depletion and nodal point enhancement are independent of the parameter a. Second, for small positive a, there are short-range enhancements of the nodal density, as the nodal line for the Dirichlet case $a = 0$ migrates to small positive Y and gets distorted and, in the complex case, broken into a line of nodal points.

We envisage that the main application of these results will be to quantum billiards, in the form of perimeter corrections to the semiclassical asymptotics of nodal statistics for eigenfunctions. It should be possible in numerical experiments to detect both the long-range nodal effects (depletions and enhancements) and the short-range enhancement for small a. We are investigating this now.

The ideas employed here can be applied more widely. For example, in a recent study, independent of ours, by Bies and Heller (2002), nodal lines were investigated for classically chaotic wavefunctions near lines in the plane where particles are reflected by a smooth potential. They employed the wave

$$\psi(\mathbf{R}) = u(\mathbf{R}) + \mathrm{i}v(\mathbf{R}) = \frac{1}{\sqrt{J}} \sum_{j=1}^{J} \mathrm{Ai}\left(Y + Q_j^2\right) \exp\{\mathrm{i}(Q_j X + \phi_j)\} \tag{26}$$

where $J \gg 1$, the Q_j are transverse wavenumbers uniformly distributed over $[-\infty, \infty]$ and the ϕ_j are random phases. This 'Airyfied Gaussian random function' satisfies the time-independent Schrödinger equation for the potential Y (all constants, including energy, can be removed by scaling).

The preceding theory can be applied directly to determine the nodal statistics of (26), provided the averages in (3) are replaced (up to an irrelevant overall constant) by

$$\begin{aligned} B(Y) &= \int_0^\infty \mathrm{d}Q\, \mathrm{Ai}^2(Y+Q^2) \\ D_X(Y) &= \int_0^\infty \mathrm{d}Q\, Q^2 \mathrm{Ai}^2(Y+Q^2) \\ D_Y(Y) &= \int_0^\infty \mathrm{d}Q\, \mathrm{Ai}'^2(Y+Q^2) \\ K(Y) &= \int_0^\infty \mathrm{d}Q\, \mathrm{Ai}(Y+Q^2)\, \mathrm{Ai}'(Y+Q^2). \end{aligned} \tag{27}$$

(The first of these equations, giving the mean probability density of a random wave near a smooth boundary, has been derived before (Berry 1989).) The Y-dependence of the density of nodal lines is given by (6), and the density of nodal points by (8).

A referee has suggested that the long-range effects reported here are not present in higher dimensions. This is correct. We have calculated the density of nodal surfaces for real Gaussian random waves in three dimensions, with Dirichlet boundary conditions on the XZ plane $Y = 0$. The leading nonoscillatory terms are proportional to $1 - 1/(80Y^2)$ for $Y \gg 1$, so that the total excess nodal area, caused by the boundary, is finite rather than logarithmically divergent.

Acknowledgments

We thank William Bies and Eric Heller for sending us their paper before publication. HI acknowledges QinetiQ for financial support.

References

Berry M V 1977 Regular and irregular semiclassical wave functions *J. Phys. A: Math. Gen.* **10** 2083–91

Berry M V 1989 Fringes decorating anticaustics in ergodic wavefunctions *Proc. R. Soc.* A **424** 279–88

Berry M V 2002 Statistics of nodal lines and points in chaotic quantum billiards: perimeter corrections, fluctuations, curvature *J. Phys. A: Math. Gen.* **35** 3025–38

Berry M V and Dennis M R 2000 Phase singularities in isotropic random waves *Proc. R. Soc.* A **456** 2059–79

Berry M V and Robnik M 1986 Quantum states without time-reversal symmetry: wavefront dislocations in a nonintegrable Aharonov–Bohm billiard *J. Phys. A: Math. Gen.* **19** 1365–72

Bies W E and Heller E J 2002 Nodal structure of chaotic eigenfunctions *J. Phys. A: Math. Gen.* at press

Blum G, Gnutzmann S and Smilansky U 2002 Nodal domains statistics—a criterion for quantum chaos *Phys. Rev. Lett.* **88** 114101

Gustavson K and Abe T 1998 The third boundary condition—was it Robin's? *Math. Intelligencer* **20** 63–70

Heller E J 1991 *Chaos and Quantum Physics (Les Houches Lecture Series vol 52)* ed M-J Giannoni, A Voros and J Zinn-Justin (North-Holland: Amsterdam) pp 547–663

O'Connor P, Gehlen J and Heller E J 1987 Properties of random superpositions of plane waves *Phys. Rev. Lett.* **58** 1296–99

Saichev A I, Ishio H, Sadreev A F and Berggren K-F 2002 Statistics of interior current distributions in two-dimensional open chaotic billiards *J. Phys. A: Math. Gen.* **35** L87–L93

Wolfram S 1996 *The Mathematica Book* (Cambridge: Cambridge University Press)